

Computer-Aided Modeling, Simulation, and Exergy Analysis of Large-Scale Production of Magnetite (Fe₃O₄) Nanoparticles via Coprecipitation

Steffy J. Arteaga-Díaz, Samir Meramo, and Ángel Darío González-Delgado*

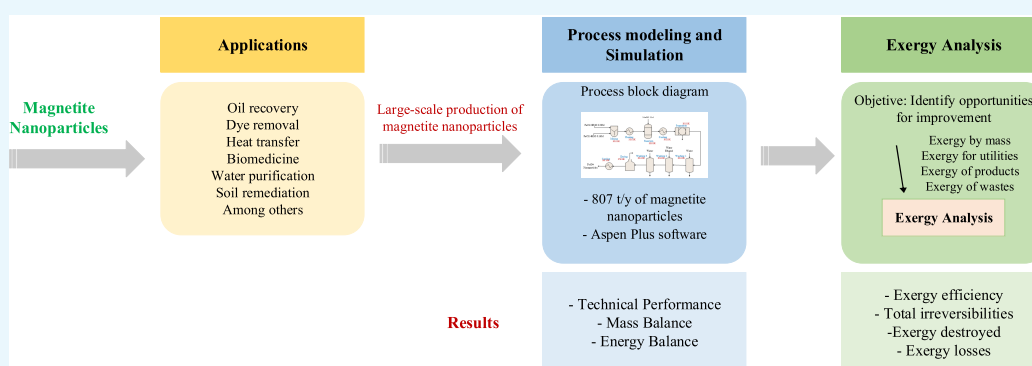
Cite This: *ACS Omega* 2021, 6, 30666–30673

Read Online

ACCESS |

Metrics & More

Article Recommendations



ABSTRACT: Magnetite nanoparticles present attractive properties including high magnetization, low toxicity, adsorption capacity, and simple preparation, making them efficient in water purification processes, soil remediation, and biomedical applications. In this sense, there is growing interest in the production of magnetite nanoparticles; therefore, evaluating the performance of this process on a large scale gives relevant information to process designers. In this work, the simulation and exergy analysis of large-scale production of magnetite nanoparticles via coprecipitation were performed using computer-aided tools. The process was modeled for the production of 807 t/year of magnetite nanoparticles; the data for the simulation were obtained from the literature, and experimental results were developed by the authors. The exergy efficiency of the process was estimated at 0.046%. The exergy of waste was estimated to be 105 313 MJ/h, while the unavoidable exergy losses were 2941 MJ/h. Washing 2 and 3 represented the most critical stages of the process, contributing 95.12% of the total irreversibilities due to the waste exergy, which corresponds to the water and ethanol exergy discarded in these stages. These results show that the process must be improved from the energy point of view and require the implementation of process optimization strategies to reach a more sustainable design.

INTRODUCTION

Iron oxide nanoparticles have attracted the scientific interest due to their application in several fields, including biomedicine, pharmaceuticals, and environment.¹ Magnetite, maghemite, and hematite are the most well-known and best-described iron oxides in the literature; however, magnetite has received more research and applications compared to other magnetic nanoparticles.² Magnetite (Fe₃O₄) is characterized by a cubic inverse spinel structure,³ which endows it with unique electrical characteristics, high magnetization, low toxicity, and adsorption strength among others,^{4,5} making them useful for photocatalytic, sonocatalytic, antibacterial, and antifungal purposes.

Regarding magnetite nanoparticles, there is considerable research on their application in the pharmaceutical industry, agriculture,⁶ water purification processes, soil remediation,⁷ and the biomedical field.^{8–10} Some of the most novel investigations include the determination of the efficiency of magnetite

nanoparticles stabilized with surfactants in the adsorption of heavy metals Cd²⁺, Pb²⁺, and Zn²⁺ from contaminated waters, as reported by Fawzia et al.⁴ Moreover, in the petroleum industry, magnetite nanoparticles tend to be of importance considering that these can be used to treat spills due to their capacity to recover oil. Elmobarak and Almomani¹¹ reported that silica-modified magnetite nanoparticles used as a demulsifier can be recovered about 90% of oil by adding 10 mg of magnetite nanoparticles per liter of emulsion; Debs et al.¹² showed in their work that magnetite nanoparticles prepared by the coprecipi-

Received: August 18, 2021

Accepted: October 18, 2021

Published: November 2, 2021



tation method have a removal capacity of over 55% for new engine oil, used engine oil, and petroleum from water, which corresponds to 218 g of oil/kg of nanoparticles. In the same sense, works suggest the efficiency of these nanoparticles in the elimination of organic dyes¹³ such as Congo red from aqueous solutions of 79.6 mg dye/g of magnetite nanoparticles, as indicated by Taher et al.¹⁴ or methylene blue with a maximum adsorption capacity of 13.54 mg/g, as shown by Anushree and Philip in their work,¹⁵ or efficiency between 72 and 89% for the removal of Optilan Blue dye from aqueous solutions, as suggested by Stan et al.¹⁶ To improve heat transfer processes, magnetite nanoparticles have also been studied. Bezaatpour and Rostamzadeh¹⁷ concluded that employing an external magnetic field with magnetite nanoparticles increases the heat transfer rate and results more efficiently compared to other methods. Likewise, Asri et al.¹⁸ synthesized ferrofluids from magnetite nanoparticles, which are used as working fluids in cylindrical heat pipes, and found excellent thermal performance.

In this sense, the application of magnetite nanoparticles in large quantities is revealed, which raises interest in their production on an industrial scale. However, there is no information in the literature on the design, assembly, and performance of a plant for the large-scale production of magnetite nanoparticles. In the laboratory, methods developed for the synthesis of these nanoparticles include the coprecipitation method, hydrothermal synthesis, solvothermal synthesis, sonochemical synthesis, and microemulsions.¹⁹ The synthesis method strongly influences the properties of the magnetite nanoparticles including size;²⁰ however, the coprecipitation method offers good control over nanoparticle size and a narrow size distribution (>25 nm).^{21,22} Therefore, the conventional method to prepare magnetite nanoparticles is via coprecipitation of ferrous and ferric ions under highly basic conditions.^{23,24} Also, this method allows the physical and chemical properties and size of the nanoparticles to be easily controlled by varying parameters such as pH, temperature, alkali type, and stirring rate.²⁵ However, large-scale technologies need to be evaluated to ensure sustainable and economically viable processes.

On this point, the modeling and simulation of the process are important, as they allow an approximation of reality;²⁶ the simulation allows us to study the effect of the modification of variables and parameters with reproducible results,²⁷ whose objective is to achieve the best configuration of the process with minimum costs, maximum efficiency, and productivity. Before carrying out the simulation, it is important to specify the objective of the model, define the mass and energy flows and the internal structure, and develop the process flow diagram. The process simulation contributes significantly to industrial development by allowing the analysis and optimization of existing processes and represents the first step in the evaluation of emerging processes under sustainability criteria. Several simulation tools or software are available, and the main ones are Aspen Plus, Aspen HYSYS, ChemCAD, Unisim Desing, SuperPro Designer, among others, which have been used successfully by different authors. For example, Oregigioni et al.²⁸ simulated the production of biomethane production from agricultural and food industry waste, and Larbi et al.²⁹ simulated the production of chitin nanomaterials; both emerging processes were simulated to analyze economic feasibility. On the other hand, Mestre-Escudero et al. simulated existing processes such as the amine treatment unit,³⁰ mercaptan oxidation unit,³¹ and sour water unit³² of a Latin American refinery to determine improvement opportunities. Therefore, the simulation of

magnetite nanoparticle production is important for predicting the technical behavior of the process at higher scales and providing information to decision makers about its technical behavior to show opportunities for improvement and to provide a technical starting point for further evaluation of the process under sustainability parameters.

It is also known that in chemical processes, exergy is destroyed by the irreversibilities derived from the second law of thermodynamics. The term exergy is defined as the maximum amount of work that can be obtained when an energy flow is moved from its initial state to the state of thermodynamic equilibrium with a reference state through reversible processes.³³ Exergy analysis has been performed by other authors to evaluate emerging technologies related to nanomaterials, for example, Meramo et al.^{34,35} performed exergy analysis for the production of TiO₂ nanoparticles via green chemistry and a process for the production of chitosan microbeads modified with nanoparticles. In this work, the simulation and exergy evaluation of large-scale production of magnetite (Fe₃O₄) nanoparticles are carried out using computer-aided tools. The information and data necessary for the simulation are obtained from the literature and experimental results obtained by the authors. The exergy analysis provides information for the sustainable implementation of this process on a large scale.

RESULTS AND DISCUSSION

The simulation of the large-scale production of magnetite nanoparticles via coprecipitation was carried out taking into account the following considerations

- The process simulation was performed at the steady state with fixed conditions such as processing capacity, process stage pressure set at 1.01 bar, and environment temperature at 301.15 K. The detailed operating conditions of each stage are summarized in Table 1.

Table 1. Operating Conditions for the Process Units of Large-Scale Production of Fe₃O₄ Nanoparticles

stage	temperature (K)	mass flow (kg/h)
solution 1	301.15	2471.52
solution 2	301.15	2494.19
mixing	301.15	4965.71
solution 3	301.15	3505.59
heating	353.15	4965.71
reaction	353.15	8471.30
cooling 1	301.15	8471.30
separation	301.15	8471.30
washing 1	301.15	6733.04
washing 2	301.15	5928.39
washing 3	301.15	7787.79
drying	378.15	588.80
cooling 2	301.15	96.58

- The nonrandom two-liquid (NRTL) solution model for electrolytes—ELECNRTL—was selected for the process simulation, considering the polar and electrolytic nature of the substances involved in the process.
- The mixing and solution preparation units were simulated in stirred tanks.
- The reactor was simulated using an RStoic model for 98% conversion.

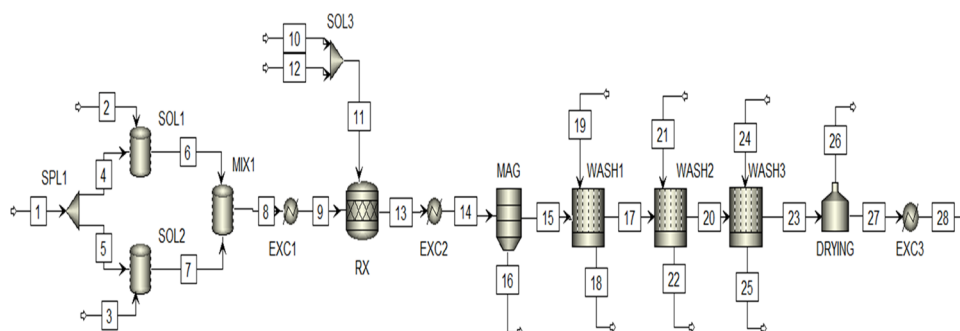


Figure 1. Simulation of large-scale production of Fe_3O_4 nanoparticles.

- The magnetic separation stage was modeled as a membrane to retain solid nanoparticles.
- The washing stages were simulated as manipulator blocks.
- The drying of nanoparticles was simulated using a direct contact oven.

The simulation of large-scale production of magnetite nanoparticles is shown in Figure 1. $\text{FeCl}_3 \cdot 6\text{H}_2\text{O}$ (stream 2) and $\text{FeCl}_2 \cdot 4\text{H}_2\text{O}$ (stream 3) are fed to SOL1 and SOL2 stages, respectively. A 0.36 M solution of $\text{FeCl}_3 \cdot 6\text{H}_2\text{O}$ and a 0.16 M solution of $\text{FeCl}_2 \cdot 4\text{H}_2\text{O}$ were prepared in these units. The two solutions (streams 6 and 7) are mixed in a stage named MIX and then sent to a heating process in the heat exchanger EXC1. The hot solution (stream 9) enters the reactor (RX) where sodium hydroxide 3 M (stream 11) is added.

NaOH acts as a precipitating agent and increases the pH of the medium to 12, allowing the formation of the magnetite nanoparticles and NaCl . Stream 13 containing the magnetite nanoparticles is sent to the EXC2 exchanger for cooling. Next, the cold stream (stream 14) undergoes a purification process comprising a separation unit (MAG), where the nanoparticles are separated from the unreacted material and NaCl , and three washing stages (WASH1, WASH2, and WASH3), in which water and ethanol are used as washing fluids. Finally, the purified nanoparticles (stream 23) are dried in DRYING and cooled in EXC3.

Table 2 lists the mass flow for the main process streams of the simulated process. For processing capacities of 1922.32 t/year for $\text{FeCl}_3 \cdot 6\text{H}_2\text{O}$ and 694 t/year for $\text{FeCl}_2 \cdot 4\text{H}_2\text{O}$, the simulation reported a production rate of 847 t/year for magnetite nanoparticles. Therefore, the total production yield was estimated to be 0.44 kg Fe_3O_4 /kg $\text{FeCl}_3 \cdot 6\text{H}_2\text{O}$.

Table 2. Operating Conditions and Mass Composition of the Main Streams for Large-Scale Production of Magnetite Nanoparticles

stream	6	7	11	13	28
T (K)	301.15	301.15	301.15	353.15	301.15
P (bar)	1.01	1.01	1.01	1.01	1.01
mass flow (kg/h)	2471.52	2494.19	3505.59	8471.3	96.58
mass fractions					
water	0.911	0.968	0.962	0.966	0
$\text{FeCl}_3 \cdot 6\text{H}_2\text{O}$	0.089	0	0	0.001	0.045
$\text{FeCl}_2 \cdot 4\text{H}_2\text{O}$	0	0.032	0	0	0.001
NaOH	0	0	0.038	0.001	0
ethanol	0	0	0	0	0
magnetite	0	0	0	0.011	0.953
NaCl	0	0	0	0.022	0

To validate the simulation results, some physicochemical properties of the magnetite nanoparticles provided by Aspen Plus software are compared with data reported in the literature; the findings are presented in Table 3. The approximation of the

Table 3. Comparison of the Properties of Magnetite Nanoparticles Obtained in Aspen Plus with Properties Reported in the Literature

property	this work	literature	accuracy (%)
heat capacity (Cal/(mol K))	36.31	36.16^{36}	99.5
relative density (g/cm^3)	5.20	5.20^{37}	100
thermal conductivity ($\text{kW}/(\text{m K})$)	0.052	0.051^{38}	98.1

properties obtained with those reported in the literature is higher than 98%, which shows that the strategies used to perform the simulation, the data packages, and the thermodynamic models selected were appropriate.

For the exergy analysis of the large-scale production of magnetite nanoparticles, Aspen Plus software provided the physical exergy of the streams, while the chemical exergy was estimated through the chemical exergy of the components at standard conditions of pressure and temperature.

The chemical exergy of the substances involved in the process was calculated, as shown in eq 10, the exergy of the pure elements was consulted in the literature, and the Gibbs energy was obtained from the simulation. Table 4 shows the chemical exergy calculated for the components involved in the process.

Table 4. Standard Chemical Exergy for Process Components

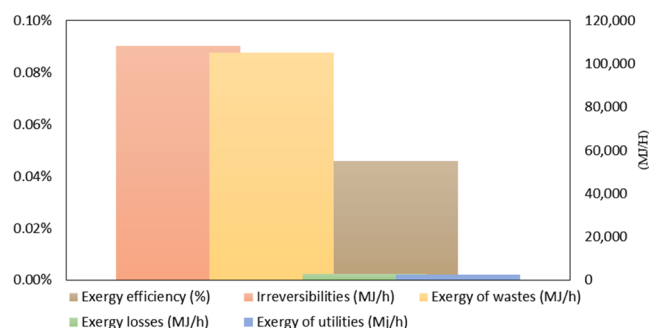
component	chemical exergy (kJ/kg)
water	50.00
$\text{FeCl}_3 \cdot 6\text{H}_2\text{O}$	843.89
$\text{FeCl}_2 \cdot 4\text{H}_2\text{O}$	1542.39
magnetite	502.30
NaCl	244.70
ethanol	27 152.16
NaOH	1875.00

The physical exergy of the streams was obtained from the process simulation, while the chemical exergy of the streams was calculated by eq 9. The physical and chemical exergies of the main process streams are presented in Table 5.

Figure 2 shows the overall results of the exergy analysis for the large-scale production of magnetite nanoparticles via coprecipitation. The total irreversibilities were estimated to be 108 254 MJ/h. The highest contribution to the irreversibilities is due to the amount of waste exergy, which represents approximately

Table 5. Chemical and Physical Exergy of the Main Streams of the Large-Scale Production of Magnetite Nanoparticles

stream	physical exergy (MJ/h)	chemical exergy (MJ/h)
2	0.00	185.06
3	0.00	77.85
6	0.26	263.98
7	0.27	184.47
11	1.42	374.66
13	171.08	440.65
15	0.08	66.65
23	0.11	1981.67
28	0.00	49.88

**Figure 2.** Overall exergy analysis for the production of magnetite nanoparticles via coprecipitation.

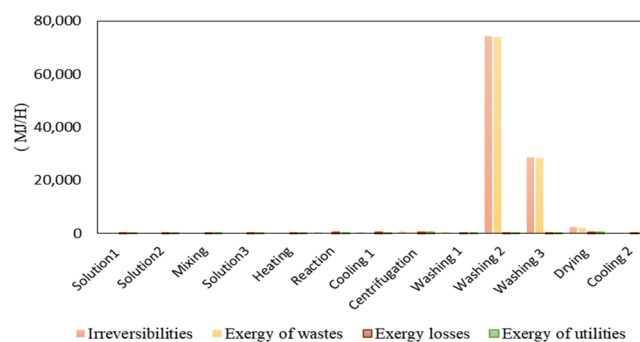
97% of the total exergy destroyed, while the unavoidable exergy losses were estimated to be 2941 MJ/h. These findings indicate that the processing units have less unavoidable exergy destruction; therefore, it is possible to achieve a thermodynamically more efficient process through the utilization of waste.

The global exergy efficiency was calculated to be 0.046%, a significantly low value for a chemical process. However, these results are related to those obtained for other emerging technologies evaluated such as large-scale production of TiO₂ nanoparticles³⁴ that reached an exergy efficiency of 0.27%, production of chitosan microbeads modified with TiO₂ nanoparticles,³⁹ and production of thiourea-modified chitosan microbeads³⁵ with exergy efficiencies of 0.044 and 3%, respectively.

The low exergy efficiency of the process is mainly attributed to the exergy destroyed with waste. Therefore, it is important to implement strategies for technological improvements, redesign of the stages, and inclusion of additional units for waste recovery to obtain a more efficient process from the exergy point of view.

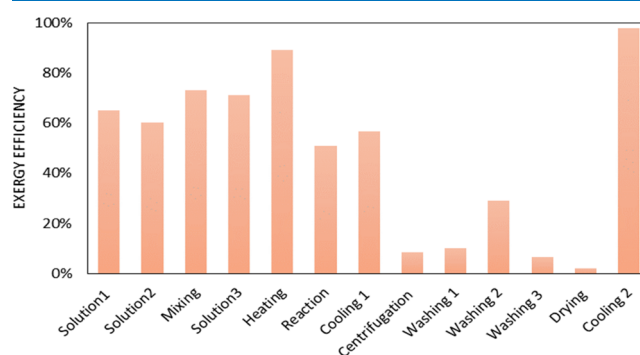
Figure 3 presents the results of the exergy analysis per stage for the large-scale production of magnetite nanoparticles via coprecipitation. The results reveal that the most critical units of the process are washing 1 and 3 for reaching the highest irreversibilities (74 214 and 28 754 MJ/h, respectively). The irreversibilities in these stages are given mainly by the exergy of waste; therefore, it is stated that the destruction of exergy in the washing units is due to the amount of water and ethanol discarded. Moreover, the input exergy of washing 2 represents approximately 96% of all of the input exergy, which can be explained by the entrance of a large amount of ethanol, whose chemical exergy is notably higher compared to the other chemical substances involved in the process; therefore, this stage has a higher significance on the overall exergy efficiency.

Water and ethanol can be treated for reuse as washing fluids, thus reducing irreversibilities and achieving energy improve-

**Figure 3.** Exergy analysis per stage for the large-scale production of magnetite nanoparticles via coprecipitation.

ment in the process. On the other hand, it was found that the exergy for industrial services is significantly low in all of the units, which indicates low heat and work required in the processing stages.

As shown in Figure 4 the stages with the highest exergy efficiency are the heating and cooling units and solution 1

**Figure 4.** Exergy efficiency per stage for the large-scale production of magnetite nanoparticles via coprecipitation.

(65%), solution 2 (60%), mixing (73%), and solution 3 (71%). These results indicate that there is no destruction of exergy by waste; therefore the exergy destroyed is only related to the unavoidable exergy losses. On the other hand, the lowest exergy efficiencies are identified in the drying, washing 3, washing 1, and washing 2 stages with efficiencies of 1.96, 6.45, 10.05, and 28.97%, respectively.

Figure 5 shows the Sankey diagram for the large-scale production process of magnetite nanoparticles by the coprecipitation method. This figure shows the contribution of each stage to the total irreversibilities (percentage of exergy destroyed) and the influence of each stage on the overall exergy efficiency. For the magnetite nanoparticle production process, it is found that the stage that contributes the most irreversibilities is washing 2 (68.55%) followed by washing 3 (26.562%), which confirms the results of the exergy analysis per stage. The stages with minimum contribution to irreversibilities are solution 1 (0.131%), solution 2 (0.113%), solution 3 (0.142%), and mixing (0.152%). To reduce the irreversibilities of magnetite nanoparticle production via coprecipitation, the reuse of washing fluids is mainly recommended or else elimination of the use of ethanol.

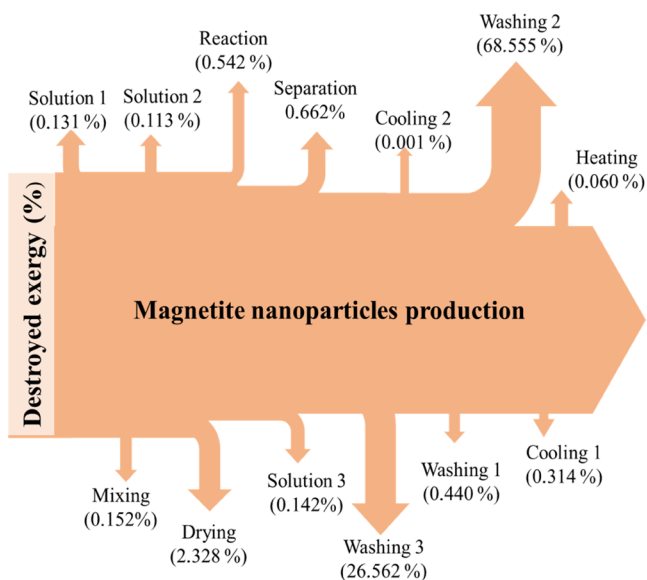


Figure 5. Sankey diagram of irreversibilities for the large-scale production of magnetite nanoparticles via coprecipitation.

CONCLUSIONS

In this work, large-scale production of magnetite nanoparticles via coprecipitation was simulated and the exergy analysis was developed to identify improvement opportunities from the exergy point of view. The route was simulated using Aspen Plus software for an annual production of 807 tons of magnetite nanoparticles. The exergy efficiency of the process was estimated to be 0.046%, suggesting that the process is inefficient. The irreversibilities of the process were due to the exergy destroyed with the residues. Washing units 2 and 3 represent the most critical stages with a contribution of 95.12% to the total irreversibilities attributable to water and ethanol discarded in these stages. Unavoidable losses in the process were estimated to be 2,941 MJ/h, considerably low compared to the exergy of waste. Therefore, it is mainly recommended to evaluate strategies for the utilization of washing fluids.

MATERIALS AND METHODS

This section covers the modeling and simulation of the large-scale production of magnetite (Fe_3O_4) nanoparticles based on the data obtained by the authors during the synthesis of the nanoparticles at a laboratory scale, and the exergy analysis of large-scale production of magnetite nanoparticles according to the methodology presented by Peralta-Ruiz et al.⁴⁰

Process Modeling and Simulation. A large-scale process was developed for the production of 807 t/year of magnetite nanoparticles. The production capacity was established by taking into account the limitations in the availability of the limiting raw material of the alternative process to coprecipitation (synthesis of magnetite nanoparticles by the green chemistry method)⁴¹ to establish a common basis for the comparison of both processes in further studies.

The process simulation is performed using Aspen Plus software following the steps listed below.

1. The chemicals involved in the process are selected from the database of the software. Aspen Plus software is characterized by an extensive, flexible, and reliable property database containing a large collection of properties of many chemicals.³⁴ For this case, all of the chemicals were available in the software database.
2. An appropriate thermodynamic model and equation of state are chosen to provide an accurate estimate of the physicochemical properties of the chemicals.
3. Input parameters such as mass/energy flow rates, temperature, pressure, and stoichiometry of the reactions are introduced.⁴²

Process Description. Figure 6 shows the process diagram for the large-scale production of magnetite nanoparticles via coprecipitation. A 0.36 M solution of $\text{FeCl}_3 \cdot 6\text{H}_2\text{O}$ and a 0.16 M solution of $\text{FeCl}_2 \cdot 4\text{H}_2\text{O}$ are fed to the process in a 2:1 molar ratio.⁴³ The solutions are mixed and undergo a heating process to increase the temperature to 80 °C.⁴⁴ Next, the mainstream goes to the reactor where a 3 M solution of NaOH is added; NaOH acts as a precipitating agent and increases the pH of the

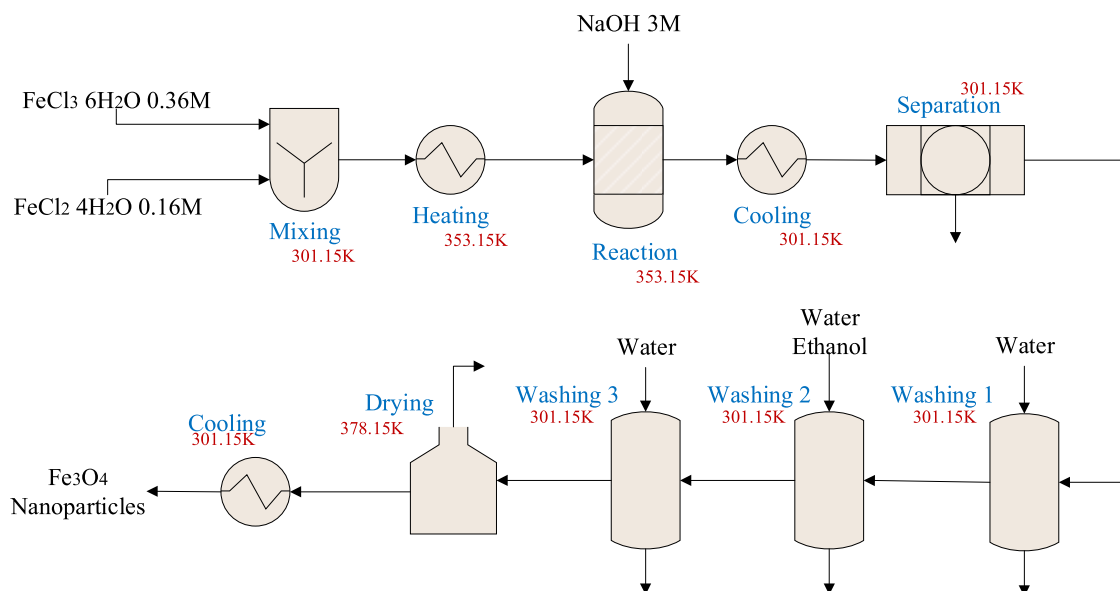
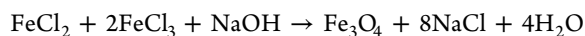
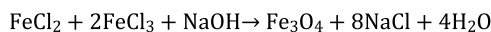


Figure 6. Process diagram of large-scale production of Fe_3O_4 nanoparticles via coprecipitation.

medium to 12, leading to the magnetite nanoparticle formation reaction (see Scheme 1).



Scheme 1. Reaction of Magnetite (Fe₃O₄) Nanoparticle Formation



The stream from the reactor is cooled to room temperature and sent to a magnetic separator where the magnetite nanoparticles are collected and separated from the remaining material. Next, the nanoparticle stream is washed in three stages using water and ethanol⁴⁵ and finally dried. Magnetite nanoparticles obtained via coprecipitation usually have a size distribution in the 25–500 nm range with high purity.⁴⁶

Exergy Analysis. Exergy analysis is an important tool for evaluating existing and emerging processing pathways from energetic and thermodynamic viewpoints.⁴⁷ Exergy analysis provides key indicators such as exergy losses, irreversibilities, percentage of exergy destroyed, and exergy efficiency that allow implementing process improvements;⁴⁸ these indicators can be calculated for each stage or the entire system.

The exergy analysis is governed by eqs 1–15. The irreversibilities indicate the unused potential work and correspond to the exergy destroyed with the waste and the unavoidable exergy losses according to the second law of thermodynamics. The irreversibilities associated with the exergy of waste can be avoided using the waste as an additional product or byproduct of the process. The destroyed exergy or irreversibilities are calculated by eq 1.

$$\dot{E}x_{\text{destroyed}} = \dot{E}x_{\text{total,in}} - \sum \dot{E}x_{\text{product}} \quad (1)$$

The unavoidable exergy losses correspond to the irreversibilities derived from the entropy increase of the thermodynamic systems; these are calculated as the difference between the total input exergy and the total output exergy, as shown in eq 2.

$$\dot{E}x_{\text{loss}} = \dot{E}x_{\text{total,in}} - \dot{E}x_{\text{total,out}} \quad (2)$$

The total exergy input to a system is associated with the mass flows entering the system (process streams) and the industrial services required (mechanical work, heating, cooling, among others). The total input exergy is calculated by eq 3.

$$\dot{E}x_{\text{total,in}} = \sum \dot{E}x_{\text{mass,in}} + \sum \dot{E}x_{\text{utilities}} \quad (3)$$

The total exergy output of a system is associated with the mass flows of the product and waste streams and is defined by eq 4.

$$\dot{E}x_{\text{total,out}} = \sum \dot{E}x_{\text{product}} + \sum \dot{E}x_{\text{wastes}} \quad (4)$$

The exergy related to mass flow in the absence of electrical, magnetic, nuclear, and surface tension effects is calculated by eq 5. Kinetic exergy ($\dot{E}x_{\text{kin}}$) and potential exergy ($\dot{E}x_{\text{pot}}$) tend to be neglected due to the low contribution to the total exergy.

$$\dot{E}x_{\text{mass}} = \dot{E}x_{\text{phy}} + \dot{E}x_{\text{chem}} - \dot{E}x_{\text{pot}} - \dot{E}x_{\text{kin}} \quad (5)$$

Physical exergy ($\dot{E}x_{\text{phy}}$) is defined by eq 6, relating enthalpy (\dot{H}) and entropy (\dot{S}) to the operating conditions and enthalpy (\dot{H}_0) and entropy (\dot{S}_0) to the reference conditions. For gases and the solid–liquid mixture, this equation is transformed into eqs 7 and 8, respectively.

$$\dot{E}x_{\text{phy}} = (\dot{H} - \dot{H}_0) + T_0(\dot{S} - \dot{S}_0) \quad (6)$$

$$\dot{E}x_{\text{phy}} = C_p(T - T_0) - T_0 \left(C_p \ln \frac{T}{T_0} - R \ln \frac{P}{P_0} \right) \quad (7)$$

$$\dot{E}x_{\text{phy,liq-sol}} = C_p \left[(T - T_0) - T_0 \ln \frac{T}{T_0} \right] - v_m(P - P_0) \quad (8)$$

where C_p is the heat capacity, v_m is the molar volume, P is the operating pressure, and P_0 is the reference pressure.

The chemical exergy ($\dot{E}x_{\text{chem}}$) is calculated by eq 9, where $\dot{E}x_{\text{ch},i}^0$ is the chemical exergy of component i in the mixture, y_i is the mole fraction of component i , and R is the universal constant of the gases. The chemical exergy of each component is calculated by eq 10, where n_j is the number of atoms of element j in component i , $\dot{E}x_{\text{ch},i}^0$ is the chemical exergy of element j , and $\Delta G_{f,i}^0$ is the Gibbs free energy.

$$\dot{E}x_{\text{chem}} = \sum_i y_i \dot{E}x_{\text{ch},i}^0 + RT_0 \sum_i y_i \ln(y_i) \quad (9)$$

$$\dot{E}x_{\text{ch},i}^0 = \Delta G_{f,i}^0 + \sum_j n_j \dot{E}x_{\text{ch},j}^0 \quad (10)$$

The exergy of utilities is defined by eq 11. The exergy by heat ($\dot{E}x_{\text{heat}}$) is calculated by eq 12 and involves the Carnot efficiency that represents the fraction of the energy transferred from a heat source at temperature T that can be converted into work in an environment at reference temperature T_0 . The exergy by work ($\dot{E}x_{\text{work}}$) in a system where there is no change in volume is equal to the work of the system itself (w), as indicated by eq 13.

$$\dot{E}x_{\text{utilities}} = \dot{E}x_{\text{heat}} + \dot{E}x_{\text{work}} \quad (11)$$

$$\dot{E}x_{\text{heat}} = \left(1 - \frac{T_0}{T} \right) \dot{Q} \quad (12)$$

$$\dot{E}x_{\text{work}} = \dot{W} \quad (13)$$

To calculate the exergy efficiency of a process, the exergy destruction and the total exergy inputs to the system are taken into account, as shown in eq 14; the percentage of exergy destroyed at stage i can be calculated by eq 15.

$$\eta_{\text{exergy}} = 1 - \left(\frac{\dot{E}x_{\text{destroyed}}}{\dot{E}x_{\text{total,in}}} \right) \quad (14)$$

$$\% \text{ Ex}_{\text{destroyed},i} = \left(\frac{\dot{E}x_{\text{destroyed},i}}{\dot{E}x_{\text{total,in}}} \right) \times 100 \quad (15)$$

■ AUTHOR INFORMATION

Corresponding Author

Ángel Darío González-Delgado – *Nanomaterials and Computer-Aided Process Engineering Research Group (NIPAC), Chemical Engineering Department, Faculty of Engineering, University of Cartagena, Cartagena 130014, Colombia*; orcid.org/0000-0001-8100-8888; Email: agonzalezd1@unicartagena.edu.co

Authors

Steffy J. Arteaga-Díaz – *Nanomaterials and Computer-Aided Process Engineering Research Group (NIPAC), Chemical*

Engineering Department, Faculty of Engineering, University of Cartagena, Cartagena 130014, Colombia

Samir Meramo – The Novo Nordisk Foundation Center for Biosustainability, Technical University of Denmark, Kongens Lyngby 2800, Denmark; orcid.org/0000-0002-9350-9898

Complete contact information is available at:

<https://pubs.acs.org/10.1021/acsomega.1c04497>

Author Contributions

S.J.A.-D., S.M., and A.D.G.-D. conceived and designed the paper. S.J.A.-D. and S.M. wrote the introduction and materials and methods. S.M., S.J.A.-D., and A.D.G.-D. wrote the results and prepared figures and tables. Discussion and conclusions were the collective work of all authors. The writing review & editing was performed by A.D.G.-D. A.D.G.-D. supervised the development of this paper.

Notes

The authors declare no competing financial interest.

ACKNOWLEDGMENTS

The authors thank the Colombian Ministry of Science, Technology and Innovation Minciencias, for its support with project “Removal of polycyclic aromatic hydrocarbons (PAHs), present in coastal waters Cartagena Bay by using shrimp exoskeleton as a source of nanoparticle-modified bioadsorbents”, code 1107748593351 CT069/17 and the University of Cartagena for supplying equipment and software necessary to conclude successfully this research.

REFERENCES

- (1) Iannone, F. M.; Groppa, M. D.; Zawoznik, S. M.; Coral, D. F.; Fernández, M. B.; Benavides, M. P. Magnetite nanoparticles coated with citric acid are not phytotoxic and stimulate soybean and alfalfa growth. *Ecotoxicol. Environ. Saf.* **2021**, *211*, No. 111942.
- (2) Strakhov, I. S.; Mezhev, Y. O.; Korshak, Y. V.; Kovarskii, A. L.; Shtil, M. Preparation of Magnetite Nanoparticles Modified with Poly(o-phenylenediamine) and Their Use as Drug Carriers. *Russ. J. Appl. Chem.* **2016**, *89*, 447–450.
- (3) Kumar, A.; Gupta, M. Synthesis and surface engineering of iron oxide nanoparticles for biomedical applications. *Biomaterials* **2005**, *26*, 3995–4021.
- (4) El-dib, F. I.; Mohamed, D. E.; El-shamy, O.; Mishrif, M. R. Study the adsorption properties of magnetite nanoparticles in the presence of different synthesized surfactants for heavy metal ions removal. *Egypt. J. Pet.* **2020**, *29*, 1–7.
- (5) Fajaro, F.; Setyawan, H.; Widiyastuti, W.; Winardi, S. Synthesis of magnetite nanoparticles by surfactant-free electrochemical method in an aqueous system. *Adv. Powder Technol.* **2012**, *23*, 328–333.
- (6) Sadanandan, A.; Ramesh, M.; Saravanan, M.; Krishnan, R.; Bharathi, S.; Nataraj, D. Iron oxide nanoparticles to an Indian major carp, Labeo rohita: Impacts on hematology, iono regulation and gill Na⁺/K⁺ ATPase activity. *J. King Saud Univ., Sci.* **2015**, *27*, 151–160.
- (7) Lei, C.; Sun, Y.; Tsang, D.; Lin, D. Environmental transformations and ecological effects of iron-based. *Environ. Pollut.* **2017**, *232*, 10–30.
- (8) Zhang, H.; Malik, V.; Mallapragada, S.; Akinc, M. Synthesis and characterization of Gd-doped magnetite nanoparticles. *J. Magn. Magn. Mater.* **2017**, *423*, 386–394.
- (9) Ahmadzadeh, E.; Rowshan, F. T.; Hosseini, M. A biological method for in-situ synthesis of hydroxyapatite-coated magnetite nanoparticles using *Enterobacter aerogenes*: Characterization and acute toxicity assessments. *Mater. Sci. Eng.* **2017**, *73*, 220–224.
- (10) Mohammadi, H.; Nekobahr, E.; Akhtari, J.; Saeedi, M.; Akbari, J.; Fathi, F. Synthesis and characterization of magnetite nanoparticles by

co-precipitation method coated with biocompatible compounds and evaluation of in-vitro cytotoxicity. *Toxicol. Rep.* **2021**, *8*, 331–336.

(11) Elmobarak, W. F.; Almomani, F. Application of Fe₃O₄ magnetite nanoparticles grafted in silica (SiO₂) for oil recovery from oil in water emulsions. *Chemosphere* **2021**, *265*, No. 129054.

(12) Debs, K. B.; Cardona, D. S.; da Silva, H. D. T.; Nassar, N. N.; Carrilho, E. N. V. M.; Haddad, P. S.; Labuto, G. Oil spill cleanup employing magnetite nanoparticles and yeast-based magnetic bionanocomposite. *J. Environ. Manage.* **2019**, *230*, 405–412.

(13) Muthukumar, T.; Philip, J. A facile approach to synthesis of cobalt ferrite nanoparticles with a uniform ultrathin layer of silicon carbide for organic dye removal. *J. Mol. Liq.* **2020**, *317*, No. 114110.

(14) Taher, T.; Putra, R.; Rahayu, N.; Lesbani, A. Preparation of magnetite-nanoparticle-decorated NiFe layered double hydroxide and its adsorption performance for congo red dye removal. *Chem. Phys. Lett.* **2021**, *777*, No. 138712.

(15) Anushree, C.; Philip, J. Efficient removal of methylene blue dye using cellulose capped Fe₃O₄ nanofluids prepared using oxidation-precipitation method. *Colloids Surf., A* **2019**, *567*, 193–204.

(16) Stan, M.; Lung, I.; Soran, M. L.; Opris, O.; Leostean, C.; Popa, A.; Copaciu, F.; Lazar, M. D.; Silipas, T.; et al. Starch-coated green synthesized magnetite nanoparticles for removal of textile dye Optilan Blue from aqueous media. *J. Taiwan Inst. Chem. Eng.* **2019**, *100*, 65–73.

(17) Bezaatpour, M.; Rostamzadeh, H. Heat transfer enhancement of a fin-and-tube compact heat exchanger by employing magnetite ferrofluid flow and an external magnetic field. *Appl. Therm. Eng.* **2020**, *164*, No. 114462.

(18) Asri, N. S.; Tetuko, A. P.; Esmawan, A.; Addin, M.; Setiadi, E. A.; Putri, W. B. K.; Giting, M.; Sebayang, P. Syntheses of ferrofluids using polyethylene glycol (PEG) coated magnetite (Fe₃O₄), citric acid, and water as the working liquid in a cylindrical heat pipe. *Nano-Struct. Nano-Objects* **2021**, *25*, No. 100654.

(19) Akbarzadeh, A.; Davaran, S. Magnetic nanoparticles: preparation, physical properties, and applications in biomedicine. *Nanoscale Res. Lett.* **2012**, *7*, No. 144.

(20) Ruíz-Baltazar, Á.; Reyes-López, S. Y.; Mondragón-Sánchez, M. de L.; Robles-Cortés, A. I.; Pérez, R. Eco-friendly synthesis of Fe₃O₄ nanoparticles: Evaluation of their catalytic activity in methylene blue degradation by kinetic adsorption models. *Results Phys.* **2019**, *12*, 989–995.

(21) Bahadur, A.; Saeed, A.; Shoaib, M.; Iqbal, S.; Bashir, M. I.; Waqas, M.; Hussain, M. N.; et al. Eco-friendly synthesis of magnetite (Fe₃O₄) nanoparticles with tunable size: Dielectric, magnetic, thermal and optical studies. *Mater. Chem. Phys.* **2017**, *198*, 229–235.

(22) Songvorawit, N.; Tuitemwong, K.; Tuitemwong, P. Single Step Synthesis of Amino-Functionalized Magnetic Nanoparticles with Polyol Technique at Low Temperature. *ISRN Nanotechnol.* **2011**, *11*, 1–6.

(23) Petcharoen, K.; Sirivat, A. Synthesis and characterization of magnetite nanoparticles via the chemical co-precipitation method. *Mater. Sci. Eng. B* **2012**, *177*, 421–427.

(24) Schwaminger, S. P.; Bauer, D.; Fraga-García, P.; Wagner, F. E.; Berensmeier, S. Oxidation of magnetite nanoparticles: impact on surface and crystal properties. *CrystEngComm* **2017**, *19*, 246–255.

(25) Sahoo, Y.; Goodarzi, A.; Swihart, M. T.; Ohulchanskyy, T. Y.; Kaur, N.; Furlani, E. P.; Prasad, P. N. Aqueous ferrofluid of magnetite nanoparticles: Fluorescence labeling and magnetophoretic control. *J. Phys. Chem. B* **2005**, *109*, 3879–3885.

(26) Koulouris, A.; Misailidis, N.; Petrides, D. Applications of process and digital twin models for production simulation and scheduling in the manufacturing of food ingredients and products. *Food Bioprod. Process.* **2021**, *126*, 317–333.

(27) Himmelblau, D. M.; Bischoff, K. B. *Análisis y simulación de procesos*; John Wiley & Sons, Inc., 1976. REverte, editor.

(28) Oreggioni, G. D.; Luberti, M.; Reilly, M.; Kirby, M. E.; Toop, T.; Theodoro, M.; Tassou, S. Techno-economic analysis of bio-methane production from agriculture and food industry waste. *Energy Procedia* **2017**, *123*, 81–88.

- (29) Larbi, F.; García, A.; del Valle, L. J.; Hamou, A.; Puiggali, J.; Belgacem, N.; Bras, J. Simulation basis for a techno-economic evaluation of chitin nanomaterials production process using Aspen Plus software. *Data Brief*. **2018**, *20*, 1556–1560.
- (30) Leal-Navarro, J.; Mestre-Escudero, R.; Puerta-Arana, A.; León-Pulido, J.; González-Delgado, Á. D. Evaluating the Exergetic Performance of the Amine Treatment Unit in a Latin-American Refinery. *ACS Omega* **2019**, *4*, 21993–21997.
- (31) Mestre-Escudero, R.; Puerta-Arana, A.; González-Delgado, Á. D. Process Simulation and Exergy Analysis of a Mercaptan Oxidation Unit in a Latin American Refinery. *ACS Omega* **2020**, *5*, 21428–21436.
- (32) Mestre-Escudero, R.; Puerta-Arana, A.; González-Delgado, Á. D. Assessment of a sour water treatment unit using process simulation, parametric sensitivity, and exergy analysis. *ACS Omega* **2020**, *5*, 23654–23661.
- (33) Pérez Zúñiga, D. L.; Luna Barrios, E. J.; Peralta-Ruiz, Y. Y.; González-Delgado, A. D. Techno-economic sensitivity of bio-hydrogen production from empty palm fruit bunches under colombian conditions. *Ital. Assoc. Chem. Eng.* **2016**, *52*, 1117–1122.
- (34) Meramo-Hurtado, S.; Moreno-Sader, K.; Gonzalez-Delgado, A. D. Computer-aided simulation and exergy analysis of TiO₂ nanoparticles production via green chemistry. *PeerJ*. **2019**, *7*, No. e8113.
- (35) Meramo-Hurtado, S.; Herrera-Barros, A.; González-Delgado, Á. Evaluation of large-scale production of chitosan microbeads modified with nanoparticles based on exergy analysis. *Energies* **2019**, *12*, No. 1200.
- (36) Westrum, E. F.; Grønvold, F. Magnetite (Fe₃O₄) Heat capacity and thermodynamic properties from 5 to 350 K, low-temperature transition. *J. Chem. Thermodyn.* **1969**, *1*, 543–557.
- (37) Noval, V. E.; Puentes, C. O.; Carriazo, J. G. An inorganic structure with many applications for heterogeneous catalysis Abstract Magnetita (Fe₃O₄). *Rev. Colomb. Quím.* **2017**, *46*, 42–59.
- (38) Mølgaard, J.; Smeltzer, W. W. Thermal conductivity of magnetite and hematite. *J. Appl. Phys.* **1971**, *42*, 3644–3647.
- (39) Meramo-Hurtado, S.; Urbina-Suaréz, N.; González-Delgado, Á. Computer-aided environmental and exergy analyses of a large-scale production of chitosan microbeads modified with TiO₂ nanoparticles. *J. Clean. Prod.* **2019**, *237*, No. 117804.
- (40) Peralta-Ruiz, Y.; González-Delgado, A. D.; Kafarov, V. Evaluation of alternatives for microalgae oil extraction based on exergy analysis. *Appl. Energy* **2013**, *101*, 226–236.
- (41) Patiño-Ruiz, D.; Sánchez-Botero, L.; Tejada-Benitez, L.; Hinestroza, J.; Herrera, A. Green synthesis of iron oxide nanoparticles using Cymbopogon citratus extract and sodium carbonate salt: Nanotoxicological considerations for potential environmental applications. *Environ. Nanotechnol. Monit. Manage.* **2020**, *14*, No. 100377.
- (42) Do, T. X.; Lim, Y.; Yeo, H. Techno-economic analysis of biooil production process from palm empty fruit bunches. *Energy Convers. Manage.* **2014**, *80*, 525–534.
- (43) Tao, K.; Dou, H.; Sun, K. Interfacial coprecipitation to prepare magnetite nanoparticles: Concentration and temperature dependence. *Colloids Surf., A* **2008**, *320*, 115–122.
- (44) Alfaro, I.; Molina, L.; González, P.; Gaete, J.; Valenzuela, F.; Marco, J. F.; Sáez, C.; Basualto, C. Silica-coated magnetite nanoparticles functionalized with betaine and their use as an adsorbent for Mo(VI) and Re(VII) species from acidic aqueous solutions. *J. Ind. Eng. Chem.* **2019**, *78*, 271–283.
- (45) Yazdani, F.; Edrissi, M. Effect of pressure on the size of magnetite nanoparticles in the coprecipitation synthesis. *Mater. Sci. Eng.* **2010**, *171*, 86–89.
- (46) Hadadian, Y.; Sampaio, D. R. T.; Ramos, A. P.; Carneiro, A. A. O.; Mozaffari, M.; Cabrelli, L. C.; Pavan, T. Synthesis and characterization of zinc substituted magnetite nanoparticles and their application to magneto-motive ultrasound imaging. *J. Magn. Magn. Mater.* **2018**, *465*, 33–43.
- (47) Singh, G.; Singh, P. J.; Tyagi, V. V.; Barnwal, P.; Pandey, A. K. Exergy and thermo-economic analysis of ghee production plant in dairy industry. *Energy* **2019**, *167*, 602–618.
- (48) Meramo-Hurtado, S.; Alarcón-Suesca, C.; González-Delgado, Á. D. Exergetic sensibility analysis and environmental evaluation of chitosan production from shrimp exoskeleton in Colombia. *J. Clean. Prod.* **2020**, *248*, No. 119285.